TISSUE ENGINEERING: Part A
Volume 26, Numbers 5 and 6, 2020

DOI: 10.1089/ten.tea.2019.0201

termis
Tissue Engineering
& Regenerative Medicine
International Society

ORIGINAL ARTICLE

Three Dimensional Bioprinting of a Vascularized and Perfusable Skin Graft Using Human Keratinocytes, Fibroblasts, Pericytes, and Endothelial Cells

Tânia Baltazar, PhD,[1] Jonathan Merola, MD, PhD,[2] Carolina Catarino, MS,[3,4] Catherine B. Xie, MS,[1] Nancy C. Kirkiles-Smith, PhD,[1] Vivian Lee, PhD,[5] Stephanie Hotta, MS,[6] Guohao Dai, PhD,[5] Xiaowei Xu, MD, PhD,[7] Frederico C. Ferreira, MBA, PhD,[8] W. Mark Saltzman, PhD,[9] Jordan S. Pober, MD, PhD,[1] and Pankaj Karande, PhD[3,4]

Multilayered skin substitutes comprising allogeneic cells have been tested for the treatment of nonhealing cutaneous ulcers. However, such nonnative skin grafts fail to permanently engraft because they lack dermal vascular networks important for integration with the host tissue. In this study, we describe the fabrication of an implantable multilayered vascularized bioengineered skin graft using 3D bioprinting. The graft is formed using one bioink containing human foreskin dermal fibroblasts (FBs), human endothelial cells (ECs) derived from cord blood human endothelial colony-forming cells (HECFCs), and human placental pericytes (PCs) suspended in rat tail type I collagen to form a dermis followed by printing with a second bioink containing human foreskin keratinocytes (KCs) to form an epidermis. *In vitro*, KCs replicate and mature to form a multilayered barrier, while the ECs and PCs self-assemble into interconnected microvascular networks. The PCs in the dermal bioink associate with EC-lined vascular structures and appear to improve KC maturation. When these 3D printed grafts are implanted on the dorsum of immunodeficient mice, the human EC-lined structures inosculate with mouse microvessels arising from the wound bed and become perfused within 4 weeks after implantation. The presence of PCs in the printed dermis enhances the invasion of the graft by host microvessels and the formation of an epidermal rete.

Keywords: skin, tissue engineering, bioprinting, regenerative medicine, microvasculature

Impact Statement

Three Dimensional printing can be used to generate multilayered vascularized human skin grafts that can potentially overcome the limitations of graft survival observed in current avascular skin substitutes. Inclusion of human pericytes in the dermal bioink appears to improve both dermal and epidermal maturation.

Introduction

The combined annual incidence of skin ulcers in the United States due to venous stasis, diabetes, or pressure is estimated at 7 million individuals[1] and will increase with greater life-expectancy and increasing prevalence of diabetes. Susceptible patients often have impaired wound healing. Cutaneous wounds that do not heal may directly cause disability and serve as portals for local and systemic infectious complications.[2] Current treatments include both

Departments of [1]Immunobiology and [2]Surgery, Yale School of Medicine, New Haven, Connecticut.
[3]Center for Biotechnology and Interdisciplinary Studies and [4]Howard P. Isermann Department of Chemical and Biological Engineering, Rensselaer Polytechnic Institute, Troy, New York.
[5]Department of Bioengineering, Northeastern University, Boston, Massachusetts.
[6]Department of Biochemistry and Molecular Biology, University of Southern Denmark, Odense, Denmark.
[7]Department of Pathology and Laboratory Medicine, University of Pennsylvania School of Medicine, Philadelphia, Pennsylvania.
[8]Department of Bioengineering and Institute of Bioengineering and Biosciences, Instituto Superior Técnico, Universidade de Lisboa, Lisbon, Portugal.
[9]Department of Biomedical Engineering, Yale University, New Haven, Connecticut.

topical wound therapies/dressings and skin grafting.[3] Autologous skin grafting, while effective, creates new wounds at harvest sites that also heal poorly in these individuals.[4,5] Allogeneic skin can provide wound closure, but triggers vigorous rejection by the patient's immune system.[6]

Tissue-engineered multilayered skin grafts, such as Apligraf™, are a third treatment option. Apligraf is an engineered bilayered structure containing an epidermis with human keratinocytes (KCs) and a dermis with neonatal foreskin fibroblasts (FBs).[7] The clinical experience and basis for FDA approval is that Apligraf functions as a source of growth factors that enhance healing.[7–9] However, it sloughs over a matter of weeks. Interestingly, although the cellular constituents of Apligraf are allogeneic to the host, graft loss does not appear to be an immune-mediated rejection of these cells and does not sensitize the recipient's immune system to them.

Notably, Apligraf and other approved bilayered skin replacements lack a dermal vasculature preventing long-term stable engraftment. Our experience with recellularized dermis suggested that engineering a dermal vasculature into a bilayered skin substitute will promote stable integration of these grafts.[10] In addition, human vascular cells can provide angiocrine factors that promote healing and tissue maturation.[11,12]

A significant advance in tissue engineering over the last decade has been the advent of 3D bioprinting, an adaptation from tools developed for nonliving systems that has enabled the precise fabrication of living systems over multiple and relevant length scales.[13–15] The complexity of skin microvasculature and other three-dimensional structures that are present in human skin are difficult to replicate *in vitro* through simple manual fabrication methods.

Bioprinting approaches such as inkjet, microextrusion, and laser-assisted printing are currently being explored in the development of more complex synthetic skin models.[16–19] Recently, Huang *et al.* used a 3D bioprinting platform as a tool to promote differentiation and regeneration of sweat gland cells.[15] The authors demonstrated that a gelatin and alginate-based scaffold can create an environment capable of inducing differentiation of epidermal progenitor cells into sweat gland cells. In addition, the matrix induced sweat gland regeneration when it was directly printed on burn wounds in mice.[20]

Incorporation of pigment-producing melanocytes and immune cells in printed skin structures has also been reported.[21–23] Other approaches using 3D bioprinting technology have shown to successfully generate perfusable capillary-like structures *in vitro*.[24,25] Despite these advances, there are still major limitations in the generation of functional endothelial networks of physiologically relevant dimensions *in vitro*. To our knowledge, the lowest diameter reported of a 3D bioprinted perfused vessel in a skin construct was of 80 μm.[26] This size is significantly larger than the capillaries found in the skin microvasculature (<26 μm at the superficial horizontal plexus and <50 μm at the dermal-subcutaneous plexus).[27,28]

We have previously demonstrated the feasibility of using 3D bioprinting to fabricate a skin equivalent.[29] However, this bioprinted skin tissue lacked a fully matured *stratum corneum* and a vascularized dermis. In this study, we demonstrate the fabrication of a multilayered, vascularized skin construct using human cells and 3D printing technology that becomes perfused through both graft and host microvessels after implantation on immunodeficient mice.

Materials and Methods

Cell isolation, culture, phenotyping, and modulation

Preliminary *in vitro* experiments were performed with human dermal FBs and KCs cultured from freshly discarded human foreskin under protocols approved by the University of Pennsylvania Institutional Review Board. Subsequent experiments used freshly discarded human foreskin obtained at Yale under protocols approved by the Yale University Institutional Review Board. FBs and KCs were isolated from foreskin samples according to previously published protocols.[30] FBs obtained from the dermis and KCs obtained from the epidermis were cultured in Dulbecco's modified Eagle's medium (DMEM; Gibco) supplemented with 10% fetal bovine serum (Atlanta Biologics), 1% Pen/Strep (Gibco), and KGM Gold medium (Lonza), respectively. Human endothelial cells (ECs) were cultured from cord blood human endothelial colony-forming cells (HECFCs) in EGM2 medium (Lonza).[31] Pericytes (PCs) were isolated and cultured in M199 medium (Gibco) supplemented with 20% fetal bovine serum and 1% Pen/Strep.[32]

Fluorescence flow cytometry confirmed that cultured dermal FBs uniformly expressed PDGFR-α, PDGFR-β, and CD90, but not NG2 (a marker of PCs), CD31 (a marker of ECs), or CD45 (a marker of hematopoietic cells). In addition, immunofluorescence microscopy confirmed positive staining for α-smooth muscle actin (Fig. 1A), suggesting that cultured dermal FBs used in this study display a myofibroblast-like phenotype.[33,34] Fluorescence flow cytometry confirmed human placental PCs express NG2, CD90, and PDGFR-β but lack PDGFR-α, CD31, and CD45 (Fig. 1B), and HECFC-derived ECs express CD31 but not CD45 (Fig. 1C). To allow long-term live cell visualization of endothelial networks *in vitro*, ECs were transduced with lentivirus expressing RFP according to the manufacturer's instructions (GeneCopoeia). All cells were maintained at 37°C and 5% CO_2 until printing.

Preparation of dermal and epidermal bioinks

Dermal and epidermal bioinks were designed based on a protocol previously described.[35] The ratio of KCs and FBs was optimized *in vitro* in preliminary experiments using human foreskin as a reference. The condition that did not show statistically significant differences in the thickness of suprabasal and basal layers compared to human foreskin was used to generate a 3D construct containing FBs and KCs. The ratio of PCs and ECs to FBs in the dermal compartment of printed constructs was also optimized *in vitro*. The condition that allowed stable endothelial self-assembly in vessels without regression as well the addition of the highest number of PCs without causing collagen contraction *in vitro* was selected to fabricate a 3D printed construct comprised of KCs, FBs, ECs, and PCs. Dermal bioink was formulated with 7.0×10^5/mL human FBs and, where indicated, 7.0×10^5/mL human ECs with or without 3.5×10^5/mL human PCs, suspended in a solution comprising 2.2 mL of 3.5 mg/mL of rat tail type I collagen (Corning), 150 μL of FBS (Atlanta Biologics), 290 μL of 10×pH reconstitution buffer (0.05 M NaOH, 2.2% $NaHCO_3$, and 200 mM HEPES), and 290 μL of 10×HAM-F12 medium (Gibco) with subsequent storage at 4°C to avoid gelation.

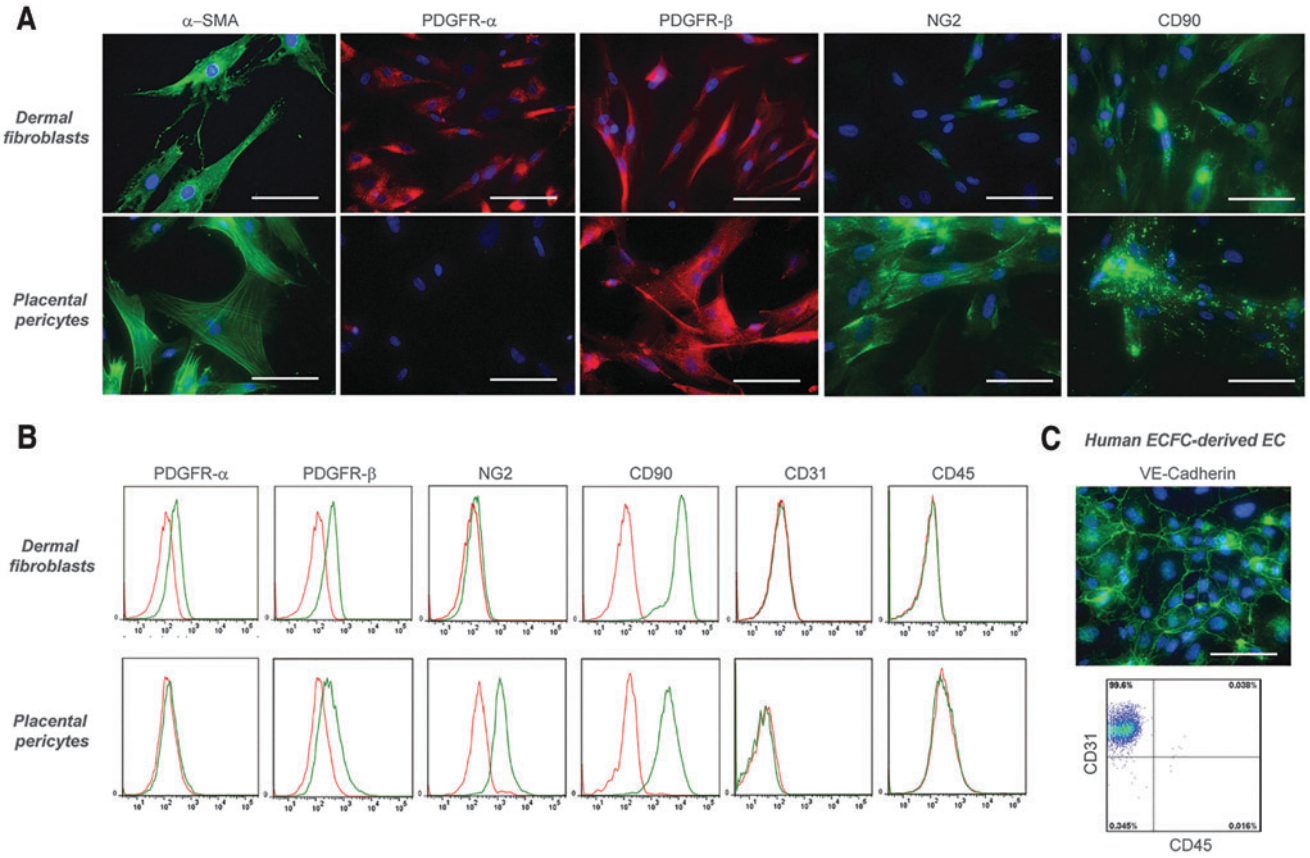

FIG. 1. Immunocharacterization and phenotyping of cultured human dermal FBs, placental PCs, and ECFC-derived ECs. **(A)** Dermal FBs express α-smooth muscle actin, PDGFR-α, PDGFR-β, and CD90 but not NG2, as confirmed by immunofluorescence microscopy. Placental PCs stained positive for α-smooth muscle actin, PDGFR-β, NG2, and CD90, but not PDGFR-α. **(B)** Flow cytometry analysis of dermal FBs confirmed the expression of PDGFR-α, PDGFR-β, and CD90. Furthermore, these cells lack expression of NG2, CD31, and CD45. PCs showed positive expression of PDGFR-β, NG2, and CD90, but lack expression of PDGFR-α, CD31, and CD45, as confirmed by flow cytometry. **(C)** Human ECFC-derived ECs stained positive for VE-cadherin by immunofluorescence microscopy and showed positive expression of CD31, but not CD45 by flow cytometry analysis. Specific staining by flow cytometry is shown in *green*; isotype-matched control staining is shown in red. Similar results were observed in three independent isolations from different donors. Scale bar: 100 μm. FB, fibroblast; PC, pericyte; ECFC, endothelial colony-forming cell. Color images are available online.

Epidermal bioink was formulated with 2×10^6/mL human KCs in 500 μL of 1:1 KGM and skin differentiation medium [DMEM/HAM's F-12 (3:1) supplemented with 10% FBS, 0.1 nM cholera toxin (Sigma), 5 μg/mL insulin (Sigma), 5 μg/mL apotransferrin (Sigma), 0.4 μg/mL hydrocortisone-21 (Sigma), and 0.5 ng/mL epidermal growth factor (Peprotech)].

Three Dimensional bioprinting of skin equivalents

Preliminary experiments to improve epidermal differentiation were conducted using a printing platform described previously.[36,37] Skin constructs were generated by printing of 2.9 mL of cold (4°C) dermal bioink containing FBs (dispensed from a 3 mL syringe), at a resolution of 300 μm and pneumatic pressure of 6 psi, on top of a six-well Transwell PET insert with 3-μm pore size. Upon gelation of dermal layers at 37°C, 500 μL of the epidermal bioink containing KCs was printed at a resolution of 300 μm and pneumatic pressure of 2.5 psi, on top of the 3D dermal construct. After printing, 1 mL of epidermal bioink without KCs was added to the bottom compartment of the six-well Transwell insert. Twenty-four hours after incubation at 37°C, the media on top and bottom of the Transwell insert were removed and changed to 100% skin differentiation medium, as described previously. After 4 days under medium submersion, the Transwell insert containing the skin equivalent was carefully transferred to air-liquid interface (ALI) on top of a 100 μm pore cell strainer placed in a Falcon® six-well Deep Well Plate (Corning). The medium on top was removed and 9 mL of skin differentiation medium was added to the bottom of the cell strainer, making sure that no bubbles were trapped under the Transwell insert. The medium below the cell strainer was replaced every 3 days for 2 weeks.

Vascularized skin grafts were fabricated using a commercially available Bio X bioprinter (CELLINK). An exchangeable print head comprising a sterile 30-gauge stainless steel blunt needle (inner ⌀: 0.15 mm; outer ⌀: 0.31 mm; CELLINK) and maintained at 4°C was used to print the dermal bioink at extrusion pressure of 50 kPa for 205 s. Bioprinted constructs were submerged in EGM2

medium for 4 days with daily medium change to allow self-assembly of endothelial networks. At day 4, a sterile 32-gauge stainless blunt needle (inner ⌀: 0.10 mm; outer ⌀: 0.24 mm; CELLINK) was used to print the epidermal bioink at extrusion pressure of 35 kPa for 54 s. Twenty-four hours later, the printed cultures were submerged in 100% skin medium for 4 additional days and were subsequently sutured on mice.

Morphological characterization of bioprinted grafts

To optimize conditions that minimize mixing of dermal and epidermal compartments, 70% confluent cultures of dermal FBs and KCs were fluorescently labeled with CellTracker™ Red CMPTX and CellTracker Green CMFDA dyes (ThermoFisher Scientific), respectively, according to the manufacturer's instructions, 24 h before printing. Three days after printing, the constructs were imaged on Nikon Eclipse Ti-E inverted fluorescence microscope (Nikon Instruments) with a motorized stage, and multiple Z-stack images were acquired to assess the spatial distribution of FBs and KCs in the printed constructs. Images were processed in NIS-Elements software (Nikon Instruments) to generate 3D projections of each sample.

Frozen sections (7 μm) of printed grafts were analyzed by H&E, immunofluorescence, and immunohistochemical staining. For immunofluorescence analysis, tissue sections were immersed in cold acetone for 10 min and blocked for 1h with 10% normal goat serum in PBS or 10% donkey serum. Slides were then incubated overnight at 4°C, in a humid chamber, with primary antibodies against cytokeratin 10 (rabbit, 1:200, clone EP1607IHCY; Abcam), cytokeratin 14 (mouse, 1:200, clone LL002; Abcam), filaggrin (mouse, 1:200, clone FLG/1561; Abcam), collagen IV (mouse; 1:200, clone COL-94; Abcam), laminin 5 (rabbit, 1:100; Abcam), ki67 (rabbit, 1:200, clone SP6; Abcam), human CD31 (mouse, 1:200, clone JC70A, Agilent), mouse F4/80 (rat, 1:50, clone BM8; eBioscience™), fluorescein Griffonia Simplicifolia Lectin I Isolectin B_4 (GSL-I B_4; 1:200; Vector Laboratories), or fluorescein Ulex Europaeus Agglutinin I (UEA-1; 1:200; Vector Laboratories). Slides were then washed with PBS (3×) and incubated for 1 h at room temperature with anti-mouse or anti-rabbit IgG H&L secondary antibodies conjugated with Alexa Fluor™ 488 or Alexa Fluor 568 (goat, 1:500; Abcam). Slides were mounted with VECTASHIELD antifade mounting medium containing DAPI (Vector Labs) for nuclear staining and imaged on a Nikon Eclipse Ti-E inverted fluorescence microscope (Nikon Instruments). Immunohistochemical analysis was performed with the following Biotin-SP AffiniPure IgG (H+L) antibodies: donkey anti-rabbit IgG (H+L), donkey anti-mouse IgG (H+L), and goat anti-rat. Substrate to the secondary antibody was included in the VECTASTAIN ABC Peroxidase Kit and AEC Peroxidase Substrate Kit (Vector Laboratories).

Engraftment of bioprinted vascularized skin in SCID/bg mice

All procedures were performed under protocols approved by the Yale Institutional Animal Care and Use Committee. Printed skin constructs were engrafted under sterile conditions onto the side of 6–12-week-old female C.B-17 SCID/bg mice (Taconic Farms, Germantown, NY) anesthetized by intraperitoneal injection of ketamine/xylazine. Mouse skin (~2 diameter) was excised from the dorsal side of the animal and a comparable-sized piece of printed skin was placed on the wound and sutured in place using 6-0 Prolene suture. The graft was then covered with two layers of Vaseline gauze, precoated with Bacitracin cream, a layer of Tegaderm, two bandages covering the size of the wound, and finally wrapped with Coban 3M tape. Bandaging was removed 10 days after implantation.

Assessment of in vivo *perfusion by tail vein injection of fluorescein UEA-I*

Fluorescein UEA I (Vector Laboratories) was diluted in a 1:1 ratio with saline solution. Two-hundred microliters were injected per mouse via the tail vein and allowed to circulate for 30 min before harvesting grafts. Mice were euthanized and grafts were harvested and cut in half: one half was fixed in 10% buffered formalin overnight for paraffin-embedding; the other half was embedded in OCT, frozen, and cryosectioned (7 μm thick).

Results

Generation and characterization of distinct epidermal/dermal compartments of bioprinted skin grafts

To enable the printing of multilayered 3D skin constructs, we previously used nebulization with $NaHCO_3$ to crosslink collagen.[29] In this model, 8 layers of collagen precursor were sequentially deposited. Between each layer of collagen and FBs, nebulized $NaHCO_3$ was applied as a crosslinking agent. We tested this gelation method to fabricate a vascularized skin graft composed of human primary cells and varied the nebulization time from 5 to 10 s. However, nebulization failed to promote homogeneous distribution of FBs within the dermis and support KC differentiation (Fig. 2A). When collagen layers were nebulized for 5 s, dermal FBs deposited at the bottom of the Transwell insert, whereas nebulization for 10 s produced a striated pattern with visible separation between the layers of FBs.

In agreement with these observations, histological analysis of the printed constructs at day 20 showed aggregation of dermal FBs near the Transwell insert membrane when collagen layers were nebulized for 5 s, while nebulization for 10 s led to spatial separation of the collagen and FBs layers. Both conditions either showed no or poor epidermal differentiation. To address this, we developed an alternative method for collagen crosslinking by mixing cells with a pH reconstitution buffer immediately before printing, with subsequent incubation at 37°C in skin differentiation medium (Fig. 2B).

Printed skin constructs were cultured at ALI starting at day 4. At day 30, these bioprinted constructs showed significant improvement in the distribution of FBs within the dermis, and improved morphology of the subsequently printed epidermal compartment (Fig. 2C), with positive epidermal staining of filaggrin (a marker of *stratum corneum*), CK14 (a marker of *stratum basal*), CK10 (a marker of suprabasal layers), and collagen type IV (a marker of basement membrane), similar to human skin. In addition, the resulting epithelium had well-organized cuboidal basal cells adherent to the basement membrane, indicative of the development of a mature skin tissue.

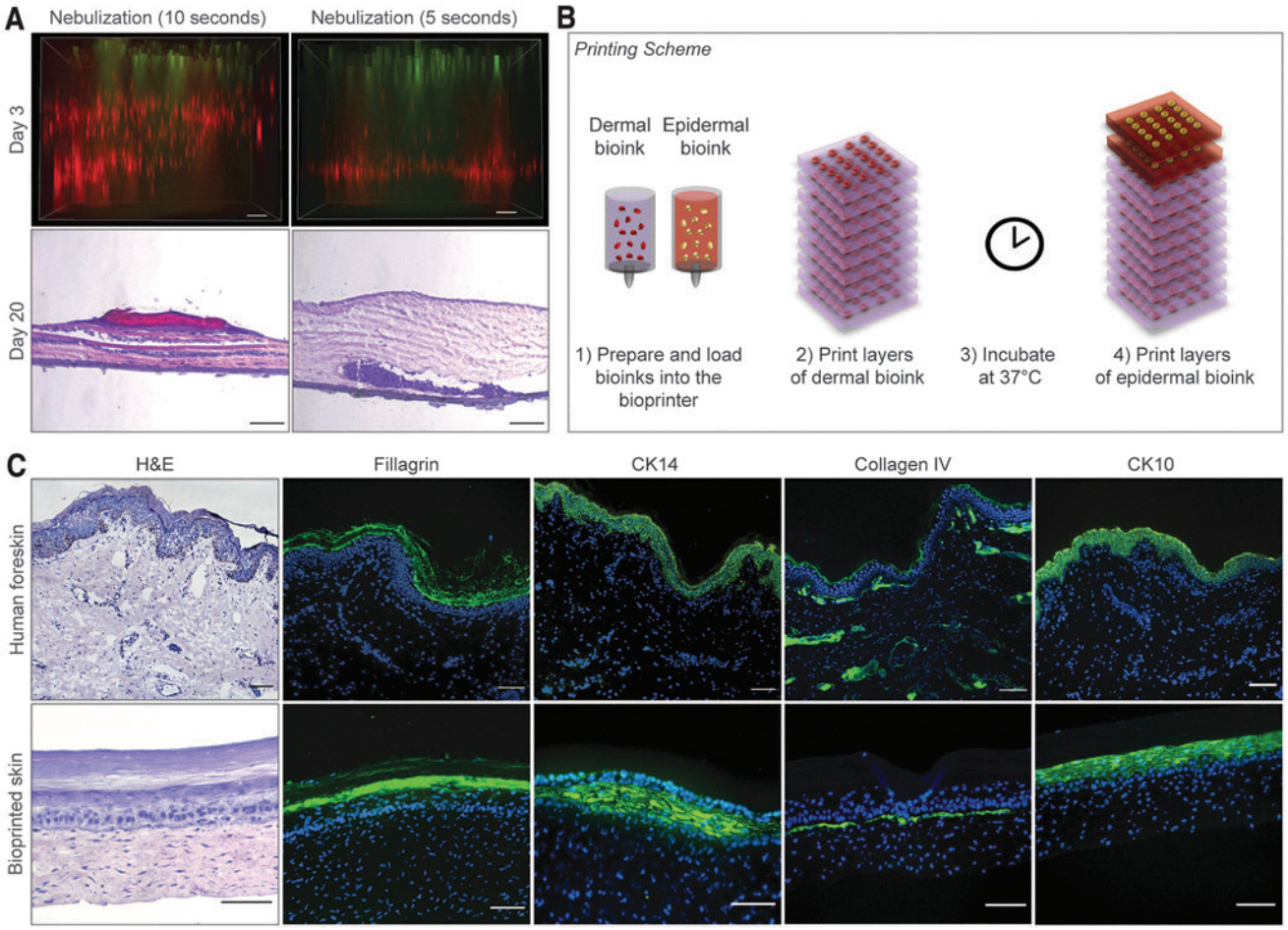

FIG. 2. Optimization, maturation, and characterization of dermal/epidermal compartments of bioprinted skin constructs *in vitro*. **(A)** Evaluation of the effect of nebulized $NaHCO_3$ as a collagen crosslinking agent on distribution of dermal FBs and differentiation of KCs in 3D bioprinted constructs. Top images are shown as maximum projections of z-stack epifluorescence images of printed constructs at day 3. FBs and KCs were fluorescently labeled with CellTracker™ *Red* CMPTX and CellTracker *Green* CMFDA dyes, respectively. *Bottom* images show H&E staining of bioprinted constructs 20 days after printing demonstrating heterogeneous distribution of FBs when collagen layers were nebulized. Scale bar: 100 μm. **(B)** Schematic showing layer-by-layer bioprinting of human skin equivalents. **(C)** Representative images of H&E and immunofluorescence staining of human foreskin and bioprinted constructs 30 days after *in vitro* maturation. Printed grafts show positive expression of filaggrin, cytokeratin 14, cytokeratin 10, and collagen type IV, similar to human foreskin. Cell nuclei were stained with DAPI (*blue*). Scale bar: 100 μm. KC, keratinocyte. Color images are available online.

Incorporation of human endothelial cells and placental pericytes into the dermal compartment of 3D bioprinted skin grafts

We assessed the ability of HECFC-derived ECs to produce vessel-like structures when incorporated in the dermal compartment of bioprinted skin grafts. We first evaluated the ability of skin differentiation medium to induce and/or maintain endothelial networks *in vitro* (Fig. 3A). Live imaging analysis of constructs cultured in skin differentiation medium did not show endothelial network formation during 4 days of culture (Fig. 3B, protocol A). In contrast, EGM2 medium during the initial culture period supported vessel self-assembly, but was not required after day 4 (Fig. 3B, protocol B).

Z-stack confocal imaging of dermal constructs in skin medium at day 10 revealed 3D endothelial networks with open lumens (Fig. 3C), which secreted collagen type IV, a principal component of the basement membrane of the capillary endothelium and were surrounded by dense collagen fibers (Supplementary Movie S1). Importantly, no signs of vessel regression were observed up to 50 days of subsequent culture in skin differentiation medium (Fig. 3D).

PCs stabilize microvessels *in vivo* and *in vitro*.[32,38] Therefore, we incorporated PCs into the dermal bioink. Seven days after bioprinting, human PCs directly associated with EC-lined vessels, while FBs remained randomly distributed within the matrix (Fig. 3C).

To generate vascularized bilayered skin constructs for implantation, dermal and epidermal compartments were printed in two stages. First, the vascularized dermal compartment was bioprinted with human ECs and FBs and cultured in EGM2 for 4 days to promote vascular self-assembly. Second, the epidermal compartment containing KCs was bioprinted on day 4 and cultured in skin differentiation medium until engraftment without exposure to an ALI (Fig. 4A). This 2-step approach allowed self-assembly of endothelial networks in the dermis as well as epidermal

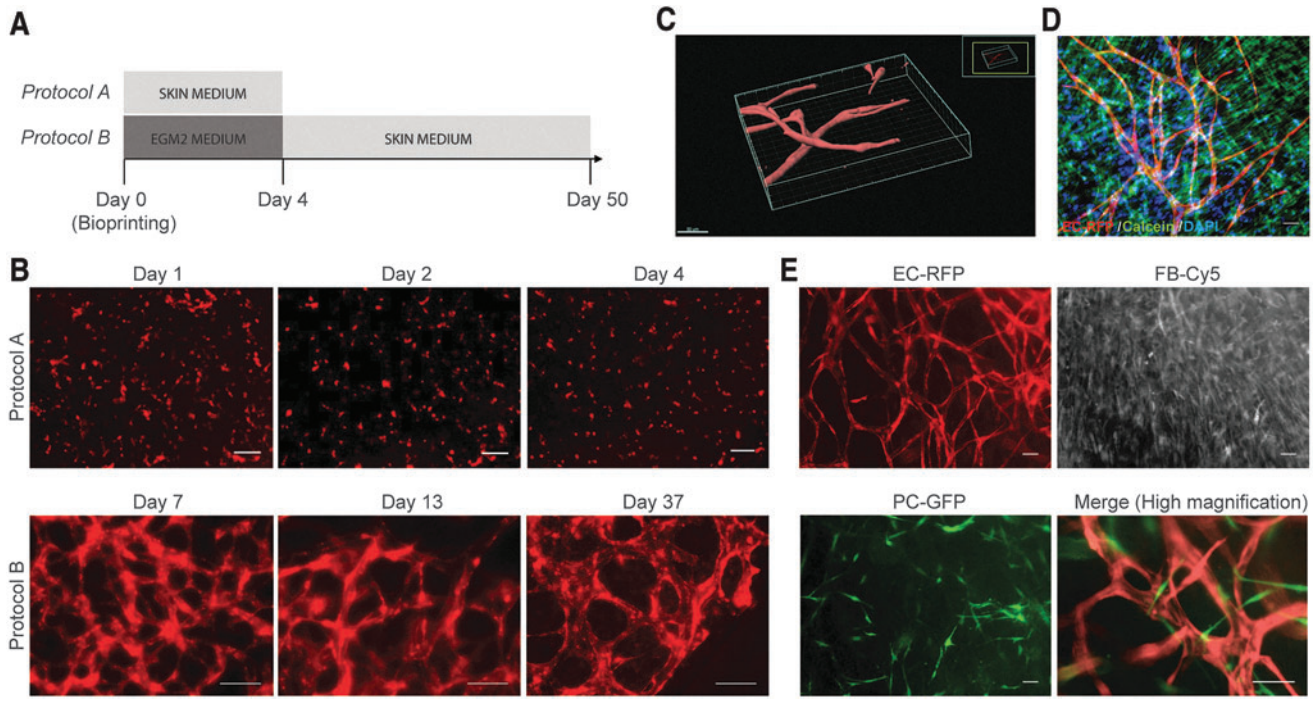

FIG. 3. Evaluation of culture conditions to allow endothelial network assembly in bioprinted dermal constructs *in vitro*. **(A)** Timeline of culture conditions tested: RFP-expressing ECs cocultured with dermal FBs in bioprinted dermal constructs cultured in skin medium for 4 days (protocol A); or EGM2 for 4 days and subsequently in skin medium until day 37 of *in vitro* culture (protocol B). **(B)** Live cell fluorescence microscopy of bioprinted dermal constructs cultured with protocol A, showing absence of EC network formation, whereas protocol B promoted self-assembly and long-term maintenance of EC networks. Scale bar: 100 μm. **(C)** 3D reconstruction of self-assembled endothelial networks in skin medium *in vitro* at day 10. Scale bar: 50 μm. Grids define the 3D space. **(D)** Printed samples were followed for 50 days to evaluate long-term endothelial network stability and viability in skin medium. Live cells were stained with calcein (*green*) and nuclei with Hoechst (*blue*). **(E)** Live imaging of cocultures of RFP-expressing ECs, Cy5-dermal FBs, and GFP-expressing PCs, 7 days after printing. Scale bar: 100 μm. Color images are available online.

keratinization. Immunohistochemical analysis of skin grafts containing ECs at day 10 showed the presence of human $CD31^+$ vessel-like structures within the dermis (Fig. 4B). As expected, bioprinted grafts without human ECs did not stain for human $CD31^+$ cells.

Similar to human skin, all bioprinted skin grafts showed positive Ki67 and CK14 expression in the epidermal basal layer, indicative of normal proliferation of basal KCs. Interestingly, in this experiment, the presence of PCs in the dermis of the skin grafts significantly increased epidermal thickness and maturation. Particularly, skin grafts containing human PCs showed increased expression of laminin 5, a principal component of the epidermal basement membrane, and presence of $CK10^+$ suprabasal terminally differentiated KCs above well-organized $CK14^+$ cuboidal basal KCs.

Characterization of 3D bioprinted skin grafted onto immunodeficient mice

Bioprinted skin grafts with and without incorporation of human ECs and PCs were implanted on the dorsal part of immunodeficient mice after 8 days of *in vitro* culture (Fig. 5A). In a pilot experiment, bioprinted skin grafts implanted for 14 days showed a high degree of hemorrhage and inflammation, particularly in nonvascularized bioprinted grafts compared to grafts containing human vascular cells (Fig. 5B). Skin substitutes formulated with human ECs and PCs contained vascular structures 2 weeks postengraftment and a higher degree of epidermal organization as shown by cytokeratin 10 and 14 expression, as well as early-stage formation of *rete ridges.*

At 30 days after engraftment, the human origin of the epidermis was assessed by involucrin staining, a marker of terminal differentiation of human KCs (Fig. 6A). Immunohistochemical analysis confirmed that the epidermis of bioprinted vascularized skin grafts was formed by human KCs. Moreover, significant contraction was observed in bioprinted grafts without ECs. Histological analysis of bioprinted grafts at day 30 confirmed that bioprinted grafts without EC were significantly smaller, and a significantly larger area was occupied by mouse skin in comparison to the grafted vascularized skin (Fig. 6B).

As expected, no human ECs were detected in grafts that did not include human ECs (Fig. 6C). Constructs formulated with human ECs contained vascular structures 4 weeks postengraftment. Some microvessels were lined by mouse ECs stained with GSL-B_4, suggesting host angiogenesis. However, many vessels distant from the wound bed were lined with human ECs (Fig. 6C). Fluorescent UEA-1 injected through the tail vein 30 min before explant labeled human ECs, confirming perfusion of these vessels. Bioprinted grafts containing PCs displayed human $CD31^+$ vessels with many surrounded by a secondary layer of CD31-negative cells.

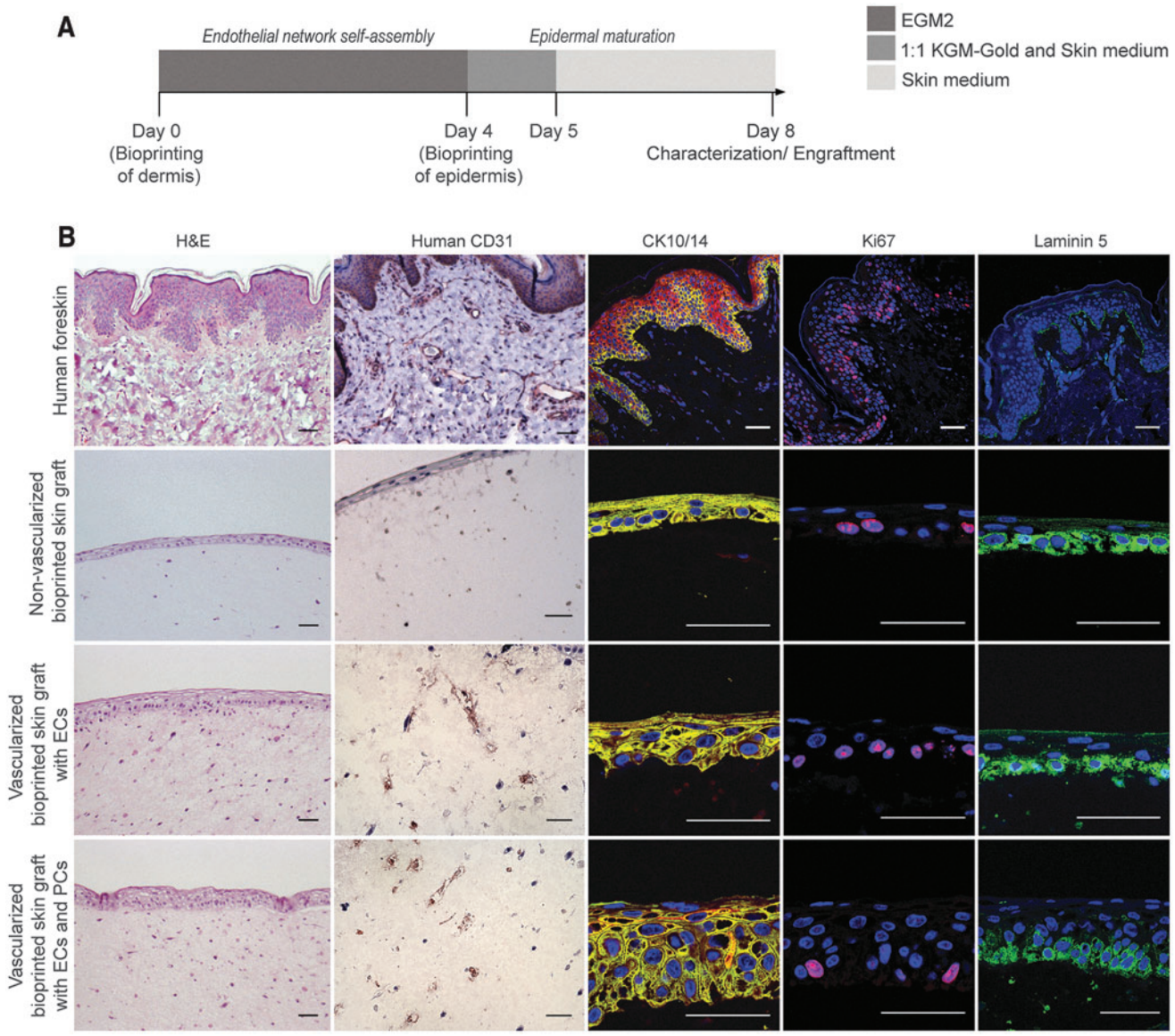

FIG. 4. Characterization of 3D bioprinted vascularized skin equivalents before engraftment. **(A)** Timeline of 2-stage protocol to fabricate human vascularized skin equivalents. First, bioprinting of a vascularized dermal compartment cultured in EGM2 for 4 days and, second, bioprinting of the epidermal compartment and culture in skin medium. At day 8, bioprinted constructs were characterized or implanted onto an immunodeficient mouse model. **(B)** Representative images of H&E and immunofluorescence staining of human adult skin and bioprinted constructs at the time of engraftment. Bioprinted skin grafts containing ECs show human $CD31^+$ vessel-like structures, whereas bioprinted grafts without human ECs do not. Bioprinted skin grafts showed positive Ki67 and CK14 expression in the epidermal basal layer. Skin grafts containing human PCs showed increased expression of laminin 5 and $CK10^+$ suprabasal terminally differentiated KCs. Cell nuclei were stained with DAPI (*blue*). Scale bar: 50 μm. Color images are available online.

The presence of a mature stratified epidermis and the formation of *rete ridge*-like structures were observed in vascularized skin grafts, particularly in grafts containing PCs. The expression of laminin 5 at the epidermal-dermal junction was also observed in all grafts. Interestingly, grafts containing PCs in addition to ECs appeared to evoke a more extensive angiogenic host response. All of the implanted grafts showed infiltration of F4/80-expressing mouse macrophages in both the wound bed and in the dermal and basal layers of the epidermis of the grafted skin. In contrast, grafts lacking ECs appeared more intensely infiltrated. Compared to the 14-day explants, the inflammation associated was reduced, suggestive of resolution.

Discussion

The absence of a vascular bed within currently available bilayered skin equivalents limits their capacity for stable engraftment as a permanent treatment for nonhealing cutaneous ulcers. In this study, we incorporated a vascular bed self-assembled from human ECs, with or without human PCs, in the dermal layer of a 3D bioprinted skin graft.

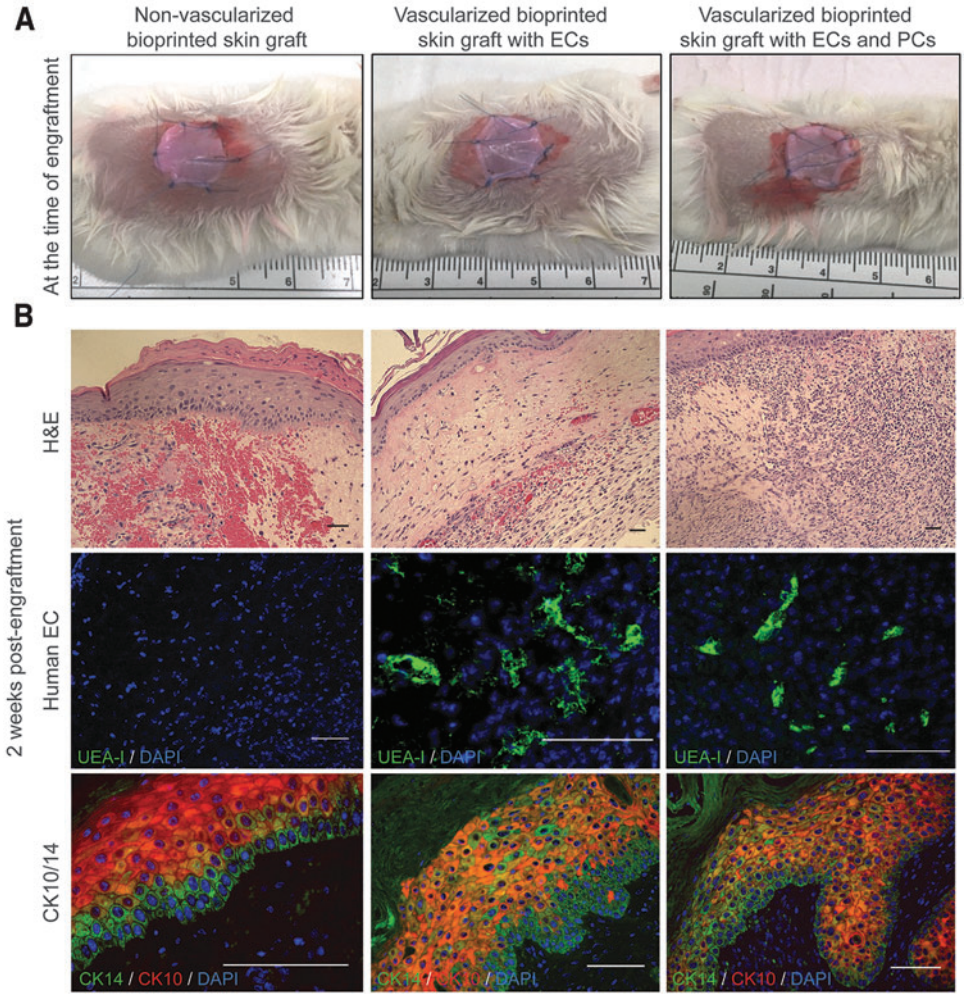

FIG. 5. Characterization of 3D bioprinted skin grafts at the time of engraftment and 2 weeks postengraftment onto immunodeficient mice. **(A)** Photographs of bioprinted grafts with and without incorporation of ECs and PCs at the time of engraftment. **(B)** Representative images of H&E and immunofluorescence staining of bioprinted constructs 2 weeks post-engraftment. H&E staining shows a higher degree of hemorrhage in non-vascularized bioprinted skin grafts compared to grafts containing ECs. UEA-1 staining shows the presence of human EC-lined vessels. Formation of rete ridges was observed particularly in vascularized bioprinted grafts containing PCs. Scale bar: 50 μm. Color images are available online.

Past approaches using 3D bioprinting technology have generated capillary-like networks by prepatterning of channels lined with ECs *in vitro*.[24,25] We used an alternate approach that focuses on self-assembly of ECs to generate prevascularized dermal compartments before engraftment. Although patterning strategies offer the advantage of an easy connection to a flow system, vessel patterning is often achieved with nonphysiological designs, and small vessel diameters are difficult to generate and perfuse.[26,39] In contrast, when ECs are allowed to self-assemble into microvessels, they form complex morphologies with patterns that resemble natural tissues with lumen diameters similar to native microvessels.[40,41]

Furthermore, we were able to demonstrate that our approach overcomes limitations related to vessel regression *in vitro* and perfusion *in vivo*.[26,42] Specifically, the incorporation of FBs and PCs mitigated vessel regression before engraftment, and the vessels were perfused *in vivo* both in an angiocrine manner (as evidenced by host vessel invasion) and through anastomosis (as evidenced by preinjected Ulex staining).

To our knowledge, the generation and implantation of a 3D bioprinted skin graft comprising a vascularized dermis with perfused human EC-lined vessels and human epidermis *in vivo* has not yet been realized. Recently, Kim *et al.* used a bioink from porcine skin-derived decellularized extracellular matrix (dECM) to bioprint a vascularized skin patch on immunodeficient mice by using both extrusion and inkjet printing modules.[43] Human adipose derived mesenchymal stem cells (ASC) and HECFC-derived ECs were loaded in dECM bioink to generate a skin patch of 1 cm diameter and 1 mm thickness. Accelerated wound closure was observed in ASC + EC-dECM encapsulated bioprinted patches due to rapid degradation of the dECM; host neovascularization and reepithelization was observed through the recruitment of host cells. Almost complete reepithelization (~90% of initial gap length) by the host was achieved after 14 days. However, the presence of perfused human EC-lined vessels within the dermis of the bioprinted skin patch was not reported.

One issue that limited our previous efforts was controlling the gelation of type I collagen in the dermal bioink.[29] We improved the distribution of dermal FBs in the bioprinted dermis by mixing a pH reconstitution buffer before printing instead of nebulization with $NaHCO_3$, which was previously used for collagen crosslinking.[29] However, under these printing conditions, mixing the collagen precursor with a pH reconstitution buffer initiates rapid crosslinking, increasing viscosity and gelation, and potentially clogging the printing assembly. We solved this problem by holding the dermal bioink at 4°C, which was accomplished with CELLINK's

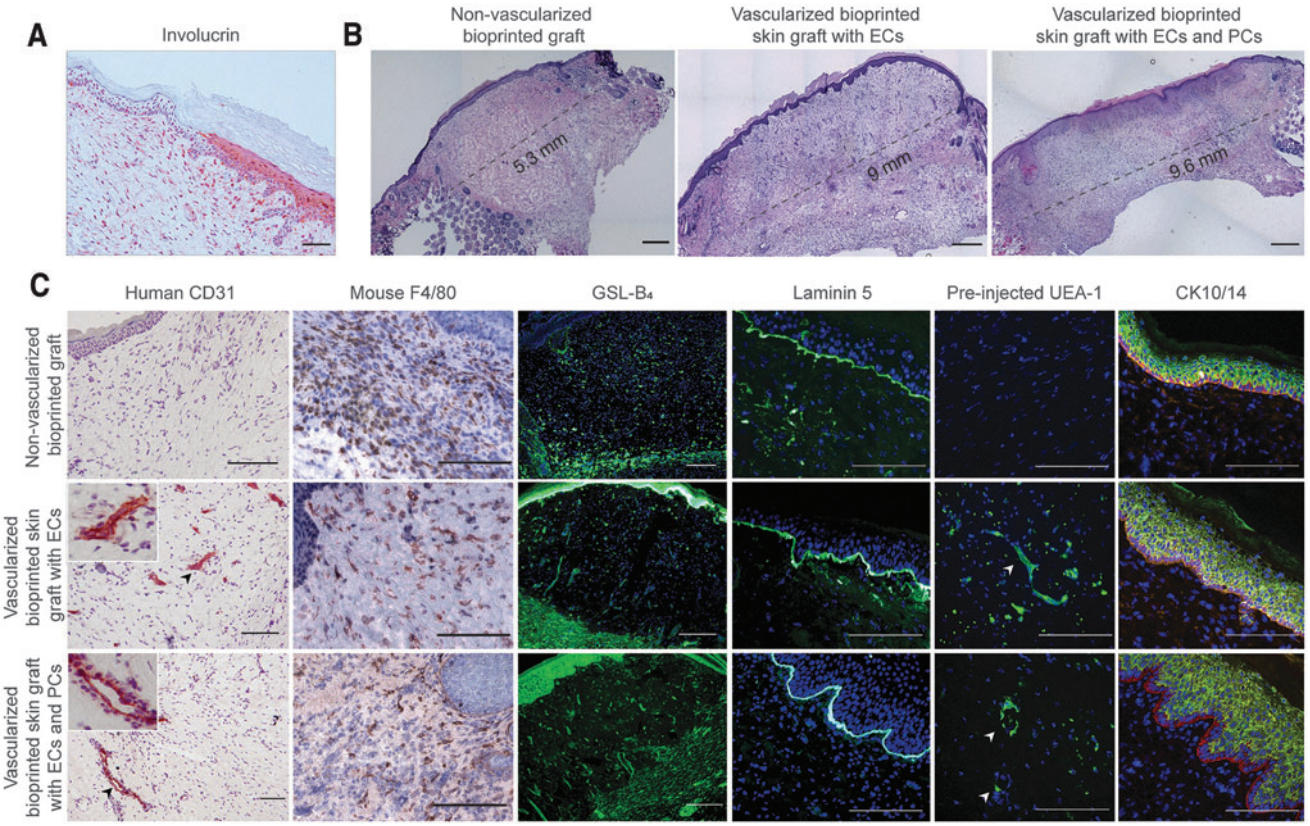

FIG. 6. Characterization of 3D bioprinted skin equivalents 4 weeks postengraftment. **(A)** Immunohistochemical staining of human involucrin, at the wound edge, showing that epidermis of 3D bioprinted vascularized skin is of human origin. Scale bar: 50 μm. **(B)** Representative H&E images of bioprinted grafts showing the extent of contraction. Bioprinted grafts without ECs and PCs were significantly smaller with a larger area occupied by the mouse skin. The border between bioprinted graft and mouse skin was identified by thin epidermis, presence of hair follicles and deep dermis with adipose tissue. Scale bar: 1 mm. **(C)** Substitutes formulated with human ECs contained vascular structures 4 weeks postengraftment. Presence of mouse microvessels and infiltration of mouse macrophages were assessed by staining with GSL-B_4 and F4/80 antibody, respectively. To demonstrate that human EC-lined vessels were perfused, fluorescent UEA-1 was injected 30 min before explant. *Arrows* point to perfused human-lined vessels. Vascularized bioprinted grafts displayed formation of *rete ridge*-like structures, particularly in bioprinted grafts containing PCs. Scale bar: 100 μm. Color images are available online.

Bio X bioprinter with an exchangeable cooled printing head, which is critical for robust, consistent, and high-throughput fabrication of multiple bioprinted skin grafts in parallel.

We find that a period of *in vitro* maturation is critical to produce skin equivalents with the degree of tissue organization observed in human skin. The skin basement membrane is important for epidermal integrity and function, including the permeability barrier, forming an adhesive interface between dermis and epidermis, and controlling cellular organization and differentiation.[44–46]

Exposure to ALI along with culture conditions necessary for maturation are often used to induce epidermal differentiation of skin equivalents,[47,48] and these approaches have also been used here. For example, bioprinted skin constructs cultured for 26 days at an ALI showed markers of epidermal stratification (CK14, CK10, and filaggrin), and positive expression of basement membrane collagen IV, indicative of mature human skin development. However, when we attempted to mature bioprinted vascularized grafts *in vitro*, ALI culture caused vessel regression and collapsing of self-assembled endothelial networks.

We believe that the significant water loss induced by ALI has a detrimental effect on self-assembly of microvascular structures. To overcome this, we adopted a 2-step approach for skin structures intended for implantation. This 2-step approach produced vessels with open lumens in the dermis as well as differentiation of basal KCs in the epidermis. Although this approach might limit the use of vascularized bioprinted constructs for *in vitro* disease modeling, we believe that it is a superior method for producing constructs for implantation and *in vivo* maturation.

When bioprinted grafts were implanted on immunodeficient mouse, the bioprinted vascularized skin grafts became perfused. Human EC-lined microvessels were present 2 and 4 weeks postengraftment. In addition, we observed rapid invasion of the host microvasculature into the grafts, particularly in grafts containing PCs in addition to ECs, which might explain the high graft survival of both non-vascularized and vascularized bioprinted grafts. In agreement with these observations, several studies have described the role of PCs in regulation of vessel guidance in angiogenesis through secretion of growth factors, such as hepatocyte growth factor,[49,50] and matrix metalloproteinases to allow EC migration.[51] Our data suggest that the inclusion of PCs in engineered grafts may improve graft survival rate.

Interestingly, we found that inclusion of PCs in the dermal bioink also improved KC maturation and formation of epidermal rete 4 weeks postengraftment. This observation is consistent with a prior report that dermal PCs can augment the paracrine effect of FBs on epithelial regeneration.[52] More specifically, organotypic cultures containing PCs displayed a thickened epidermis, highly polarized organization of cells within the basal layer and more ordered suprabasal stratification. Incorporation of dermal PCs in organotypic cultures enhanced the deposition of laminin-511/521 in the dermal-epidermal junction and expression of BMP-2 that conferred cell polarity and increased number of basal cell divisions.[53] Further work is needed to investigate the extrinsic cues provided by PCs to regulate the epidermal maturation and host angiogenesis observed here.

A potential bottleneck in skin tissue replacement is the large number of cells required to generate skin equivalents since they can be harvested only in small quantities directly from human biopsies. In addition, it may be impractical to obtain such cells from the recipient's own skin, particularly in patients with compromised recipient beds (e.g., in diabetes, thermal burns, or venous leg ulcers) or in hosts with impaired angiogenesis.[54–56]

In this study, we have shown that HECFC-derived ECs can be used to promote the vascularization and perfusion of bioprinted skin grafts. These can be easily isolated from umbilical cord blood or adult peripheral blood,[57,58] avoiding skin harvest. HECFC-derived ECs can be expanded for at least 100 population doublings,[59] allowing the generation of larger sized grafts. Furthermore, these ECs can be cloned, allowing selection after genetic modifications. This property may be important because in addition to promoting graft perfusion, human ECs can initiate immune-mediated rejection by direct presentation of nonself class I and -class II HLA proteins to circulating alloreactive effector memory T cells. This population is uniformly present in adult human peripheral blood and has been correlated with early rejection of clinical allografts and with rejection of human skin on immunodeficient mice introduced by adoptive transfer.[60]

In contrast, Apligraf, an avascular bilayered skin equivalent approved by FDA, does not induce acute rejection responses likely due to the fact that it lacks both professional antigen-presenting cells and ECs.[61–63] While grafts containing unmodified human ECs will be alloimmunogenic, this property can be eliminated from HECFC-derived ECs by CRISPR/Cas9-mediated deletion of HLA antigen expression.[64–66] We anticipate that successful engraftment of a 3D bioprinted human skin graft by incorporating allogeneic ECs without triggering rejection in the host would be of great clinical utility and the basis for the creation of an ''off-the-shelf'' clinical product.

Conclusion

The multilayered and stratified structure of skin makes it a prototypical tissue to be fabricated using 3D bioprinting. In this study, we demonstrate that 3D bioprinting can be used to fabricate vascularized human skin *in vitro* from human cells that is morphologically and biologically similar to human skin. In summary, we demonstrate the potential of using HECFC-derived ECs and placental PCs to generate an implantable skin graft comprising a perfusable microvascular system using 3D printing.

Acknowledgments

The authors thank Dr. Brigitte Arduini and Dr. Sergey Pryshchep (Rensselaer Polytechnic Institute) for assistance with cell isolation and 3D confocal microscopy. We acknowledge Dr. Silvya Stuchi Maria-Engler (University of São Paulo, Brazil) for providing help with protocols for the organotypic *in vitro* culture of skin grafts. We thank Gwendolyn Davis-Arrington and Alejandra Moncayo (Yale University) for assistance with EC isolation and placental PCs. This study was supported by funds from Center for Biotechnology and Interdisciplinary Studies, Fundação para a Ciência e a Tecnologia (individual fellowship SFRH/BD/52480/2014 awarded to Tânia Baltazar by FCT-Portugal) and Science Without Borders (individual fellowship, 203415/2014-0 Brazil awarded to Carolina Catarino by CNPq). Tania Baltazar also acknowledges prior institutional affiliations with 3, 4, and 8 where she performed portions of the work reported in this study.

Disclosure Statement

No competing financial interests exist.

Funding Information

This work is supported by a grant from the National Institutes of Health (R01-HL085416).

Supplementary Material

Supplementary Movie S1

References

1. Singer, A.J., and Clark, R.A.F. Cutaneous wound healing. N Engl J Med **341,** 738, 1999.
2. Falanga, V. Wound healing and its impairment in the diabetic foot. Lancet **366,** 1736, 2005.
3. Harding, K.G., Morris, H.L., and Patel, G.K. Healing chronic wounds. BMJ **324,** 160, 2002.
4. Falanga, V. The chronic wound: impaired healing and solutions in the context of wound bed preparation. Blood Cells Mol Dis **32,** 88, 2004.
5. Guo, S., and Dipietro, L.A. Factors affecting wound healing. J Dent Res **89,** 219, 2010.
6. Alrubaiy, L., and Kathem, K. Al-Rubaiy & Alrubaiy. Skin Substitutes: a Brief Review of Types and Clinical Applications. Oman Med J **24,** 6, 2009.
7. Griffiths, M., Ojeh, N., Livingstone, R., Price, R., and Navsaria, H. Survival of Apligraf in acute human wounds. Tissue Eng **10,** 1180, 2004.
8. Zelen, C.M., Gould, L., Serena, T.E., *et al.* A prospective, randomised, controlled, multi-centre comparative effectiveness study of healing using dehydrated human amnion/chorion membrane allograft, bioengineered skin substitute or standard of care for treatment of chronic lower extremity diabetic ul. Int Wound J **12,** 724, 2015.
9. Zaulyanov, L., and Kirsner, R.S. A review of a bi-layered living cell treatment (Apligraf) in the treatment of venous leg ulcers and diabetic foot ulcers. Clin Interv Aging **2,** 93, 2007.
10. Shepherd, B.R., Enis, D.R., Wang, F., *et al.* Vascularization and engraftment of a human skin substitute using circulating progenitor cell-derived endothelial cells. FASEB J **20,** 1739, 2006.

11. Tonnesen, M.G., Feng, X., and Clark, R.A.F. Angiogenesis in wound healing. J Invest Dermatol Symp Proc **5,** 40, 2000.
12. Dulmovits, B.M., and Herman, I.M. Microvascular remodeling and wound healing: a role for pericytes. Int J Biochem Cell Biol **44,** 1800, 2012.
13. Munoz-Abraham, A.S., Rodriguez-Davalos, M.I., Bertacco A., *et al.* 3D Printing of organs for transplantation: where are we and where are we heading? Curr Transplant Rep **3,** 93, 2016.
14. Lee, H., and Cho, D.-W. One-step fabrication of an organ-on-a-chip with spatial heterogeneity using a 3D bioprinting technology. Lab Chip **16,** 2618, 2016.
15. Huang, S., Yao, B., Xie, J., and Fu, X. 3D bioprinted extracellular matrix mimics facilitate directed differentiation of epithelial progenitors for sweat gland regeneration. Acta Biomater **32**, 170, 2016.
16. Ng, W.L., Chua, C.K., and Shen, Y.-F. Print Me An Organ! Why We Are Not There Yet. Prog Polym Sci **97**, 101145, 2019.
17. Derr, K., Zou, J., Luo, K., *et al.* Fully three-dimensional bioprinted skin equivalent constructs with validated morphology and barrier function. Tissue Eng Part C Methods **25,** 334, 2019.
18. Pourchet, L.J., Thepot, A., Albouy, M., *et al.* Human skin 3D bioprinting using scaffold-free approach. Adv Healthcare Mater **6,** 1601101, 2016.
19. Cubo, N., Garcia, M., Del Canizo, J.F., *et al.* 3D bioprinting of functional human skin: production and in vivo analysis. Biofabrication **9,** 15006, 2016.
20. Liu, N., Huang, S., Yao, B., *et al.* 3D bioprinting matrices with controlled pore structure and release function guide in vitro self-organization of sweat gland. Sci Rep **6,** 34410, 2016.
21. Ng, W.L., Qi, J.T.Z., Yeong, W.Y., and Naing, M.W. Proof-of-concept: 3D bioprinting of pigmented human skin constructs. Biofabrication **10,** 25005, 2018.
22. Min, D., Lee, W., Bae, I., *et al.* Bioprinting of biomimetic skin containing melanocytes. Exp Dermatol **27,** 453, 2018.
23. Vidal Yucha, S.E., Tamamoto, K.A., Nguyen, H., Cairns, D.M., and Kaplan, D.L. Human skin equivalents demonstrate need for neuro-immuno-cutaneous system. Adv Biosyst **3,** 1800283, 2019.
24. Hoch, E., Tovar, G.E.M., and Borchers, K. Bioprinting of artificial blood vessels: current approaches towards a demanding goal. Eur J Cardiothorac Surg **46,** 767, 2014.
25. Frueh, F.S., Menger, M.D., Lindenblatt, N., Giovanoli, P., and Laschke, M.W. Current and emerging vascularization strategies in skin tissue engineering. Crit Rev Biotechnol **8551,** 1, 2016.
26. Abaci, H.E., Guo, Z., Coffman, A., *et al.* Human skin constructs with spatially controlled vasculature using primary and iPSC derived endothelial cells. Adv Healthcare Mater **5,** 1800, 2016.
27. Braverman, I.M., and Keh-Yen, A. Ultrastructure of the human dermal microcirculation. III. The vessels in the mid- and lower dermis and subcutaneous fat. J Invest Dermatol **77,** 297, 1981.
28. Braverman, I.M., and Sibley, J. Ultrastructural and three-dimensional analysis of the contractile cells of the cutaneous microvasculature. J Invest Dermatol **95,** 90, 1990.
29. Lee, V., Singh, G., Trasatti, J.P., *et al.* Design and fabrication of human skin by three-dimensional bioprinting. Tissue Eng Part C Methods **20,** 473, 2014.
30. Pennacchi, P.C., de Almeida, M.E.S., Gomes, O.L.A., *et al.* Glycated reconstructed human skin as a platform to study the pathogenesis of skin aging. Tissue Eng Part A **21,** 2417, 2015.
31. Suarez, Y., Shepherd, B.R., Rao, D.A., and Pober, J.S. Alloimmunity to human endothelial cells derived from cord blood progenitors. J Immunol **179,** 7488, 2007.
32. Maier, C.L., Shepherd, B.R., Yi, T., and Pober, J.S. Explant outgrowth, propagation and characterization of human pericytes. Microcirculation **17,** 367, 2010.
33. Li, R., Bernau, K., Sandbo, N., *et al.* Pdgfra marks a cellular lineage with distinct contributions to myofibroblasts in lung maturation and injury response. Elife **7,** 2018.
34. Chen, Y.-T., Chang, F.-C., Wu, C.-F., *et al.* Platelet-derived growth factor receptor signaling activates pericyte-myofibroblast transition in obstructive and post-ischemic kidney fibrosis. Kidney Int **80,** 1170, 2011.
35. Brohem, C.A., da Silva Cardeal, L.B., Tiago, M., *et al.* Artificial skin in perspective: concepts and applications. Pigment Cell Melanoma Res **24,** 35, 2010.
36. Lee, W., Debasitis, J.C., Lee, V.K., *et al.* Multi-layered culture of human skin fibroblasts and keratinocytes through three-dimensional freeform fabrication. Biomaterials **30,** 1587, 2009.
37. Lee, V.K., Kim, D.Y., Ngo, H., *et al.* Creating perfused functional vascular channels using 3D bio-printing technology. Biomaterials **35,** 8092, 2014.
38. Shepherd, B.R., Jay, S.M., Saltzman, W.M., Tellides, G., and Pober, J.S. Human aortic smooth muscle cells promote arteriole formation by coengrafted endothelial cells. Tissue Eng Part A **15,** 165, 2009.
39. Hasenberg, T., Mühleder, S., Dotzler, A., *et al.* Emulating human microcapillaries in a multi-organ-chip platform. J Biotechnol **216,** 1, 2015.
40. Montaño, I., Schiestl, C., Schneider, J., *et al.* Formation of human capillaries in vitro: the engineering of prevascularized matrices. Tissue Eng Part A **16,** 269, 2010.
41. Marino, D., Luginbühl, J., Scola, S., Meuli, M., and Reichmann, E. Bioengineering dermo-epidermal skin grafts with blood and lymphatic capillaries. Sci Transl Med **6,** 221ra14, 2014.
42. Kim, B.S., Gao, G., Kim, J.Y., and Cho, D.-W. 3D cell printing of perfusable vascularized human skin equivalent composed of epidermis, dermis, and hypodermis for better structural recapitulation of native skin. Adv Healthcare Mater **8,** e1801019, 2019.
43. Kim, B.S., Kwon, Y.W., Kong, J.-S., *et al.* 3D cell printing of in vitro stabilized skin model and in vivo pre-vascularized skin patch using tissue-specific extracellular matrix bioink: a step towards advanced skin tissue engineering. Biomaterials **168,** 38, 2018.
44. Yurchenco, P.D., and Schittny, J.C. Molecular architecture of basement membranes. FASEB J **4,** 1577, 1990.
45. Breitkreutz, D., Koxholt, I., Thiemann, K., and Nischt, R. Skin basement membrane: the foundation of epidermal integrity—BM functions and diverse roles of bridging molecules nidogen and perlecan. Biomed Res Int **2013,** 179784, 2013.
46. Jayadev, R., and Sherwood, D.R. Basement membranes. Curr Biol **27,** R207–R211, 2017.
47. Frankart, A., Malaisse, J., De Vuyst, E., *et al.* Epidermal morphogenesis during progressive in vitro 3D reconstruction at the air-liquid interface. Exp Dermatol **21,** 871, 2012.
48. Pruniéras, M., Régnier, M., Woodley, D., *et al.* Methods for cultivation of keratinocytes with an air-liquid interface. J Invest Dermatol **81,** 28s, 1983.

49. Chang, W.G., Andrejecsk, J.W., Kluger, M.S., Saltzman, W.M., and Pober, J.S. Pericytes modulate endothelial sprouting. Cardiovasc Res **100,** 492, 2013.
50. Eilken, H.M., Diéguez-Hurtado, R., Schmidt, I., *et al.* Pericytes regulate VEGF-induced endothelial sprouting through VEGFR1. Nat Commun **8,** 1574, 2017.
51. Stapor, P.C., Sweat, R.S., Dashti, D.C., Betancourt, A.M., and Murfee, W.L. Pericyte dynamics during angiogenesis: new insights from new identities. J Vasc Res **51,** 163, 2014.
52. Paquet-Fifield, S., Schlüter, H., Li, A., *et al.* A role for pericytes as microenvironmental regulators of human skin tissue regeneration. J Clin Invest **119,** 2795, 2009.
53. Zhuang, L., Lawlor, K.T., Schlueter, H., *et al.* Pericytes promote skin regeneration by inducing epidermal cell polarity and planar cell divisions. Life Sci Alliance **1,** e201700009, 2018.
54. Alzahrani, H., Ammar, H., Alzahrani, A., and Shoaib, H. Healing of chronic diabetic foot ulcers with a skin substitute: patient selection is the key to success. Open J Regen Med **02,** 15, 2013.
55. Tahergorabi, Z., and Khazaei, M. Imbalance of angiogenesis in diabetic complications: the mechanisms. Int J Prev Med **3,** 827, 2012.
56. Zhang, X., Sarkar, K., Rey, S., *et al.* Aging impairs the mobilization and homing of bone marrow-derived angiogenic cells to burn wounds. J Mol Med **89,** 985, 2011.
57. Asahara, T., Murohara, T., Sullivan, A., *et al.* Isolation of putative progenitor endothelial cells for angiogenesis. Science (80-.) **275,** 964, 1997.
58. Bompais, H., Chagraoui, J., Canron, X., *et al.* Human endothelial cells derived from circulating progenitors display specific functional properties compared with mature vessel wall endothelial cells. Blood **103,** 2577, 2004.
59. Ingram, D.A., Mead, L.E., Tanaka, H., *et al.* Identification of a novel hierarchy of endothelial progenitor cells using human peripheral and umbilical cord blood. Blood **104,** 2752, 2004.
60. Al-Lamki, R.S., Bradley, J.R., and Pober, J.S. Endothelial cells in allograft rejection. Transplantation **86,** 1340, 2008.
61. Briscoe, D.M., Alexander, S.I., and Lichtman, A.H. Interactions between T lymphocytes and endothelial cells in allograft rejection. Curr Opin Immunol **10,** 525, 1998.
62. Briscoe, D.M., Dharnidharka, V.R., Isaacs, C., *et al.* The allogeneic response to cultured human skin equivalent in the hu-PBL-SCID mouse model of skin rejection. Transplantation **67,** 1590, 1999.
63. Dharnidharka, V., Briscoe, D., Isaacs, C., *et al.* Are professional antigen presenting cells, (APCS) Necessary to Initiate Graft Rejection? Transplantation **65,** 770, 1998.
64. Abrahimi, P., Qin, L., Chang, W.G., *et al.* Blocking MHC class II on human endothelium mitigates acute rejection. JCI Insight **1,** 1, 2016.
65. Abrahimi, P., Chang, W.G., Kluger, M.S., *et al.* Efficient gene disruption in cultured primary human endothelial cells by CRISPR/Cas9. Circ Res **117,** 121, 2015.
66. Merola, J., Reschke, M., Pierce, R.W., *et al.* Progenitor-derived human endothelial cells evade alloimmunity by CRISPR/Cas9-mediated complete ablation of MHC expression. JCI Insight **4,** pii: 129739, 2019.

Address correspondence to:
Pankaj Karande, PhD
Howard P. Isermann Department of Chemical and Biological Engineering
Rensselaer Polytechnic Institute
Troy, NY 12180

E-mail: karanp@rpi.edu

Received: July 31, 2019
Accepted: October 11, 2019
Online Publication Date: December 3, 2019